

We are IntechOpen, the world's leading publisher of Open Access books Built by scientists, for scientists

5,500

Open access books available

136,000

International authors and editors

170M

Downloads

Our authors are among the

154

Countries delivered to

TOP 1%

most cited scientists

12.2%

Contributors from top 500 universities



WEB OF SCIENCE™

Selection of our books indexed in the Book Citation Index
in Web of Science™ Core Collection (BKCI)

Interested in publishing with us?
Contact book.department@intechopen.com

Numbers displayed above are based on latest data collected.
For more information visit www.intechopen.com



Spectroscopy Technology: An Innovative Tool for Diagnosis and Monitoring of Wheat Diseases

Fenfang Lin, Dongyan Zhang, Xin-Gen Zhou and Yu Lei

Abstract

Diseases are among the most important factors limiting worldwide production of wheat. Accurate detection of diseases is the key to develop effective management strategies for control of these diseases. Spectroscopy-based technology can be a non-destructive, quick, efficient tool to accurately detect and monitor the occurrence and development of crop diseases. There has been an increased interest in the research and application of spectrum technology for the diagnosis and detection of wheat diseases in recent years. This book chapter provides a brief review on research advances in using spectroscopy techniques to detect wheat diseases, with a focus on the diagnosis and detection of *Fusarium* head blight, powdery mildew, and stripe rust, three important fungal diseases in wheat worldwide. Disease symptoms and traditional disease detection methods are also included. Both literature and our original research data are presented, with the section of conclusion and prospects at the end of this book chapter.

Keywords: wheat, spectroscopy, fusarium head blight, powdery mildew, stripe rust, hyperspectral, remote sensing, vegetation index, fungal disease, symptoms, sensor, *Fusarium graminearum* ss, *Blumeria graminis*, *Puccinia striiformis*

1. Introduction

Wheat (*Triticum aestivum*) is one of the most important food crops in the world [1] and is produced in large areas in many countries, especially in India, China, USA, Europe, and Latin and central America. Wheat ranks third in worldwide food crop production [2]. However, the world's population is expected to increase from 7.8 billion currently to more than 9 billion in 2050 [3]. It has been estimated that global grain production must be increased by more than 60% by 2050 to feed the increased population [4]. Therefore, enhancing wheat production through using high yielding cultivars and improved management practices plays an important role toward this goal. However, numerous diseases, especially powdery mildew (*Blumeria graminis*), brown rust (*Puccinia recondita* f. sp. *tritici*), yellow rust (*Puccinia striiformis*) and *Fusarium* diseases, pose a challenge to enhance wheat production. Furthermore, recently increased occurrence of extreme weather events pose an additional threat to the global wheat production and food security [5, 6]. Therefore, developing and implementing effective management strategies for wheat diseases is very important to reduce wheat yield and quality loss. However,

accurate and quick detection of wheat diseases is the first essential step for effective control of these diseases.

The traditional detection of wheat diseases is achieved by visual observations of farmers that require sufficient knowledge and skills of disease diagnosis or by laboratory tests using destructive sampling method. These methods are tedious, time-consuming, subjective and not suitable for large-scale monitoring. Because of the limitations of these traditional methods, remote sensing technology has gained more and more attentions of researchers since remote sensing is reliable, real-time and precise [7, 8]. There are three main types of remote sensing systems for plant disease monitoring: 1) visible and infrared spectral systems, 2) fluorescence and thermal systems, and 3) synthetic aperture radar and light detection and ranging equipment systems. Plant disease detection can be based on image or spectroscopic analysis from these sensor systems. A spectroscopy-based method has been used as a wide-ranging approach for the detection of plant diseases and other biotic stresses. Spectroscopy is an interaction of electromagnetic spectrum and matter, which is associated with the type of radiation energy, type of material, nature of interaction, and so on [9]. Examples of molecular and atomic spectroscopy include visible (VIS), infrared (IR), electrical impedance (EI), and fluorescence spectroscopy [10].

The purpose of this chapter is to introduce the readers to the application of spectroscopic techniques on wheat disease detection. This article focuses on three major wheat diseases, Fusarium head blight (FHB, *Fusarium graminearum*), powdery mildew (*Blumeria graminis*) and stripe rust (*Puccinia striiformis* f. sp. *tritici*). The FHB disease, also known as wheat scab, has become one of the most prevalent and damaging diseases in wheat. It can not only affect the normal physiological functions of wheat spikes but also produce deoxynivalenol that is detrimental to both human and animal [11]. Stripe rust and powdery mildew, belonging to foliar diseases, are among the most important diseases and occur in wheat all over the world. Powdery mildew is also one of the most deleterious diseases threatening wheat production worldwide [12]. Stripe rust of wheat is an airborne biotrophic fungal disease and has the capability of fast spread to the new regions and crop cultivars [13, 14]. Compared to leaf and stem rusts, stripe rust is more destructive [15]. Losses in yield caused by these three diseases can reach up to 50% or more depending the year and the country.

2. Principle of spectroscopy diagnosis and monitoring

Crop diseases produce a variety of symptoms and physiological changes in plant tissues, which is the basis for the physical analysis of their spectroscopy characteristics. These external and internal manifestations of diseases can produce an interaction with electromagnetic spectrum or radiation energy. The spectroscopy response of crop diseases can be detected by a specific sensor or sensors system.

All the three wheat diseases have the symptoms of lesions or pustules due to infection (**Table 1**). Single or multiple forms of destruction as illustrated in the table produce different levels of disease severity at the different growth stages, and these symptoms may superimpose or interact with each other. Apart from these visible symptoms, physiological changes appear in plants in the temporal process. For foliar diseases, their infection initially produces lesions on leaves. Without disease control, severer infection leads to the decrease of chlorophyll content and biomass in plants, even impediment of the water metabolism. Distinctive symptoms of each disease can respond in specific spectral regions. The features for a disease of interest can be color space, various fluorescence ratios, reflectance of a waveband or some


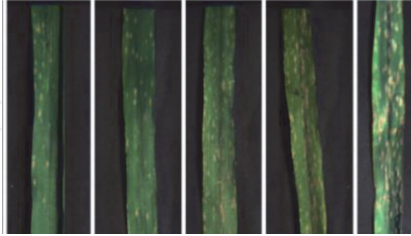

Wheat diseases	Plant damages	Symptoms
1. <i>Fusarium</i> head blight (<i>Fusarium graminearum</i> ss)	White and blighted individual spikelets or the whole spike, pink masses of spores on or in between the spikelets; the green whole crop looks green with white spikes in cases of severe infections; black hard perithecia on infected spikes at the time of harvest; pinkish and shriveled grains.	
2. Powdery mildew (<i>Blumeria graminis</i>)	White cottony mycelia with spores covering from fraction to almost the whole leaf area, the presence of cleistothecia as small black bodies (points) interlaced within the light colored at the advanced stages.	
3. Stripe rust (<i>Puccinia striiformis</i>)	The formation of uredia in a linear fashion on the leaves and yellow uredinospores on glumes.	

Table 1.
 Symptoms of three wheat diseases.

bands, spectral characteristic position variables, or some vegetation indices sensitive to the disease, which depends on the detailed exploration of spectral response mechanism for the disease. Therefore, spectroscopy monitoring can capture spectral information of diseases corresponding to different symptoms and their temporal patterns.

3. Spectroscopic systems available for diagnosing and monitoring wheat diseases

Spectroscopic information for wheat diseases detection can be color space, visible-infrared reflectance spectral and fluorescence parameters, which are derived from digital cameras, multispectral and hyperspectral sensors, and fluorescence devices. Regular digital cameras can obtain Red-Green-Blue (RGB) images with high resolution by ground mobile or Unmanned Aerial Vehicle (UAV) platforms. The leaf or spike color on RGB images is the common indicator of the health status of plants and can be used to measure the chlorophyll content. Multispectral sensors acquire data with more than three bands, including red, green, blue and near-infrared wavelengths. Health plants have high reflectance in the near-infrared region due to multiple scattering resulted from the air-cell interface of leaf inner tissue. Crop diseases can cause reflectivity variation in this region due to water deficit of plants infected with a certain degree of disease. By contrast, hyperspectral sensors have higher spectral resolution and broader wavelength range to detect the more and subtle disease information of crop. This information can indicate morphological and pathological changes of disease-infected plants in more details. Compared to reflectance spectroscopy, chlorophyll fluorescence can provide more

direct information about the physiological state of the plants, which is to measure the fluorescence from certain substances after excitation with a beam of light. Studies have found that chlorophyll fluorescence spectrum can sensitively sense plant pathogens at an early stage [16–18].

3.1 Visible digital camera system

A digital camera, covering red, green and blue bands, is the main component of the visible light camera system. It acquires images of the object of interest under the equal angle, illumination and distance. The formats of the images are JPEG, TIF, BMP, and so on. These images can be analyzed by computer vision and texture analysis techniques and plant disease information can be obtained at the image processing stage (**Figure 1**). Image preprocessing is carried out to improve image quality, such as highlighting certain features, noise removal and the enhancement of difference between the object and background. Among them, RGB images are required to convert into color space representation. These color features can be grayscale, Hue Saturation Value (HSV), Hue Saturation Intensity (HSI), Luminosity red-green-blue-yellow (LAB) or YCbCr. LAB consists of luminosity layer (L^*), chromaticity-layer (a^*), indicating the color fall along the red-green axis, and chromaticity-layer (b^*), indicating the color fall along blue-yellow axis. YCbCr is ideal for digital video images processing. In YCbCr format, Y represents luminance information while Cb and Cr are two different color information that stored color information. The originality of chromaticity can be maintained by keeping Cb and Cr constant [19]. Image segmentation is an important step for isolating the leaf or the spike from the background, followed by separating healthy tissue from diseased tissue [20]. Feature extraction involves the selection of optimal color features available for identification of wheat diseases or estimation of wheat disease index. After the features are extracted from the images, classing and staging the disease is the last task in machine vision. The common classifiers used are machine learning algorithms, such as support vector machines (SVM) and artificial neural network (ANN). Many studies have proved the effectiveness of these algorithms, achieving a high classification accuracy for plant diseases recognition under the correct selection of features and classifier parameters [21, 22]. However, success of the disease recognition algorithm depends on many variables that are subject to the judgment of the system designer, such as selection of optimal color space and suitable learning algorithm to use for classification [23]. In recent years, deep learning has been a new trend in machine learning due to its ability to exploit directly raw data without using the handcrafted features. Some studies have used deep learning models for classification between diseased and healthy plant tissues to show its potential to detect plant diseases [24, 25].

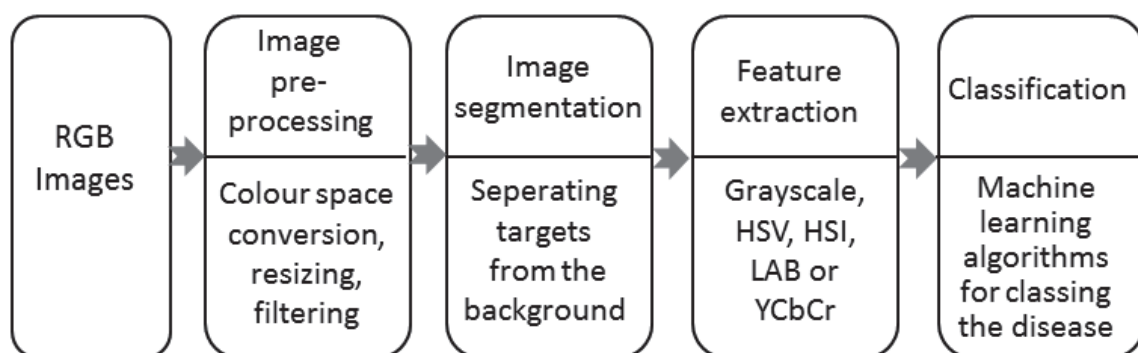


Figure 1.
A workflow for wheat disease detection by RGB images.

3.2 Visible-infrared reflectance spectroscopic system

Multispectral and hyperspectral systems introduced in this chapter are broad-band and narrow-band sensors in the visible and infrared range, respectively. These sensors are mounted on different platforms, such as ground-, aerial-, and satellite-based platforms, which can acquire imaging data with a relatively high signal-to-noise ratio. Given the fact that different symptoms and physiological changes of diseases show specific responses in the reflectance spectrum, monitoring of crop diseases mainly uses the reflected spectral information in data with various spectral resolution and spatial resolution. The general process of crop disease monitoring based on reflectance spectrum involves data preparation, spectral response mechanism analysis, optimal spectral feature selection, detecting model establishment and prevention application (**Figure 2**). Among them, the second and third steps are of importance in spectroscopy-based approaches for crop disease detection. The detailed exploration of spectral response for each disease is the basis of following feature extraction. Each disease can show absorption and reflection peaks in different wavelengths. The narrower the band width, the more obvious and subtler these features. Some sensitive wavelengths for the disease are selected through analysis of the response for construction of a new disease vegetation index. Furthermore, for specific absorption and reflection peak of the disease, a series of spectral characteristic parameters are calculated in these ranges, including position, amplitude, area, ratio and normalized ratio. Some studies show that diseases can cause spectral changes in the regions of the blue edge, green peak, yellow edge, red valley, red edge, and near-infrared. After the construction of specific and optimal indicators for the disease of interest, detecting a specific disease or retrieving the infection severity is conducted by a variety of algorithms or their combinations. For example, some statistical discriminant analysis methods have been adopted and shown good

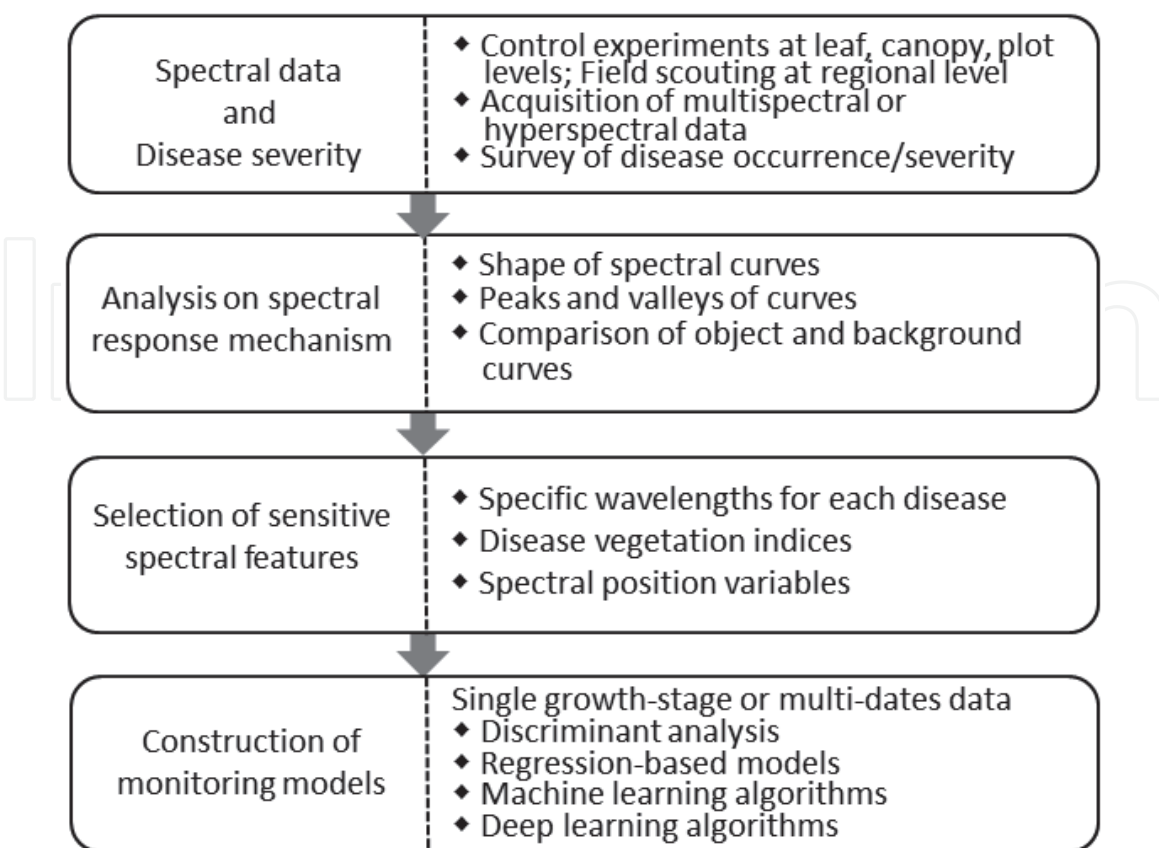


Figure 2.
 A workflow for monitoring wheat disease using the VIS-IR spectroscopic technique.

accuracy in detecting one specific disease or differentiating diseases under relatively simple scenarios [26]. And regression-based methods are widely used to determine the infection severity of plant diseases, such as multiple linear regression and partial least squares regression [27, 28]. Compared to these linear statistical methods, many machine learning algorithms, particularly deep learning approaches, have played an important role in modeling for detecting plant diseases under some complicated scenarios [24, 25]. Large amounts of data from multi-phase images can be required when damages caused by diseases are confused with some other factors. This puts forward new and high requirements for modeling.

3.3 Fluorescence spectroscopy system

Chlorophyll fluorescence, as an indicator of plant photosynthesis, can reflect the characteristics of some stresses before infection symptoms are visible, and be used in the monitoring and early warning of various physiological or non-physiological stresses [10]. Active-induced chlorophyll fluorescence techniques have been widely studied due to their strong intensity and abundant information. These fluorescence systems can obtain chlorophyll fluorescence spectrum, chlorophyll fluorescence kinetic parameters, chlorophyll fluorescence image, and life span for detecting plant stresses, such as the stresses of water, high temperature, nutrition, diseases, insect pests, and so on. Fluorescence spectroscopy devices include fiber-optic fluorescence spectrometer, imaging multispectral and hyperspectral sensors. Various ratios of fluorescence amplitude at fluorescence peaks are determined from the continuous fluorescence spectra for achieving pre-symptomatic detection for some pathogens. For example, three fluorescence ratios (F451/F522, F451/F687, F451/F736) have been used to detect early powdery mildew infection in susceptible and resistant cultivars in wheat [29]. The fluorescence spectra over 370–800 nm is also useful for pre-symptomatic detection of wheat leaf rust [30]. In addition, many types of fluorescence kinetic parameters are constructed and used based on the saturation pulse fluorescence analysis, such as the maximum quantum efficiency of photosystem II (PSII) primary photochemistry (Fv/Fm), the maximum efficiency of PSII photochemistry in light adapted material (Fv'/Fm'), non-photochemical quenching (NPQ), and the effective quantum yield of photosystem II (Φ PSII) [31, 32]. These parameters can be obtained by the continuous excitation (FRR) chlorophyll fluorescence detection system and the saturation pulse modulation (PAM) fluorescence dynamics detection system.

4. Detection and diagnosis of wheat FHB

Fusarium head blight (FHB) is a major and devastating disease of wheat worldwide. The pathogen invades wheat ears and causes damage in the kernels in the form of atrophy, weight reduction, and discoloration, resulting in significant yield and quality loss. The fungus also produces mycotoxin deoxynivalenol (DON) that could destroy healthy cells by inhibiting protein synthesis. Food and feed contaminated with DON pose a serious threat to human and animal health [33, 34]. Management practices for control of FHB and DON contamination is critical to the profitable and sustainable production of wheat. Detection and diagnosis of the development of this disease is the first but essential step toward control of it.

4.1 Hyperspectral data acquisition and assessment of disease severity

The hyperspectral images of wheat ears were acquired by the SOC710E imaging spectrometer (Surface Optics Corporation, San Diego, USA) in the field. This

imager has a spectral range of 400–1000 nm and the spectral resolution of 2.3 nm. Wheat ears in the field were cut and put on a black light-absorbing cloth. Then, the data were collected by the hyperspectral imager from 11:00 AM to 2:00 PM under fine weather conditions (**Figure 3**). The images obtained contained the front side (defined as side A) and the reverse side (defined as side B) of wheat heads for making sure the comprehensiveness of data acquisition.

After hyperspectral data collection, disease severity level (DSL) of wheat FHB was calculated according to the GBT 15796–2011 Rules for Monitoring and Forecast of the Wheat FHB.

$$DSL = \frac{W_d}{W_h} \quad (1)$$

where W_d is the number of pixels within the diseased area of the wheat ear; and W_h is the number of pixels in the whole ear after removing the wheat awn.

The lesion area in wheat ear was extracted by the binarization and morphological processing (**Figure 4**). The original images were RGB images combined by the three central wavelengths of red (660 nm), green (560 nm) and blue (480 nm) from hyperspectral images of wheat ears. The RGB image was then converted to another color space with three components of Y, Db and Dr. Finally, a threshold segmentation method was used to extract and calculate the diseased area of wheat ears.

4.2 Spectral response of wheat ears under different disease severities

In the process of using hyperspectral data to accurately identify diseases, the study of spectral signatures under different disease severities is the basis for screening and identifying sensitive bands of diseases. **Figure 5** shows the spectral response of wheat ears with different infection levels. Generally, in the range of the 550–720 nm band, the spectral reflectance of healthy ears is lower than that of infected samples, with an

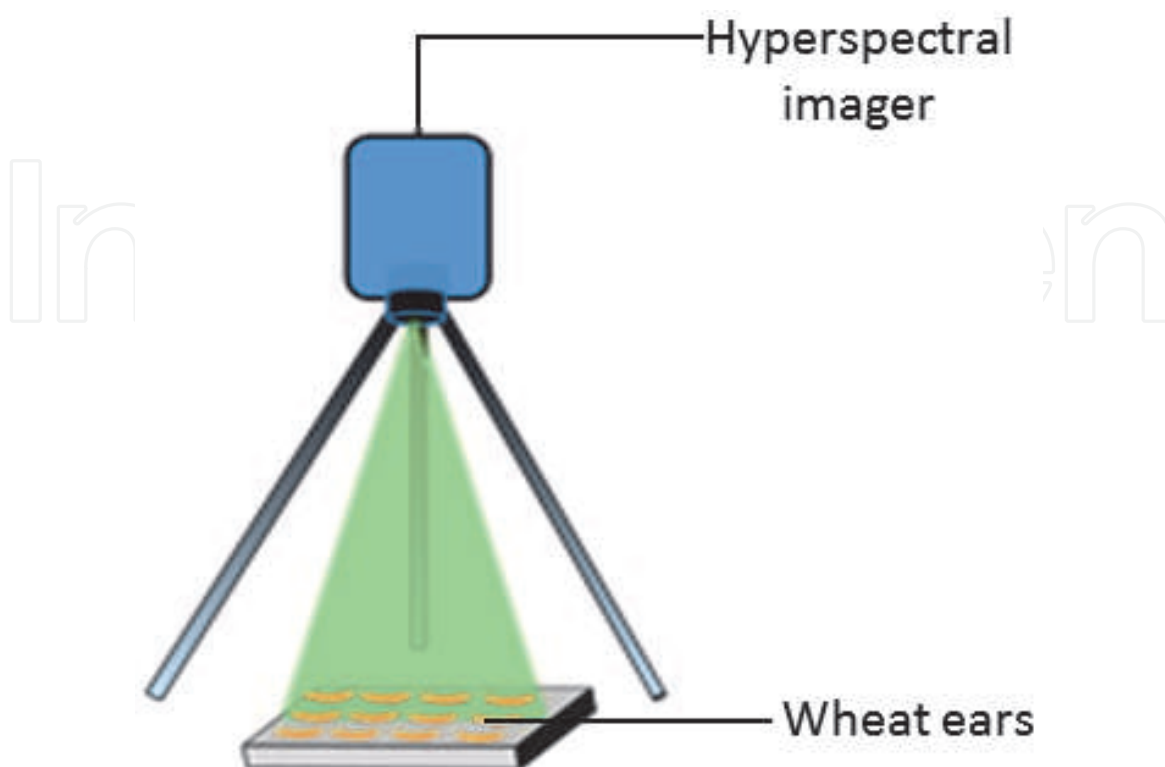


Figure 3.
Acquisition of hyperspectral images for wheat ears.

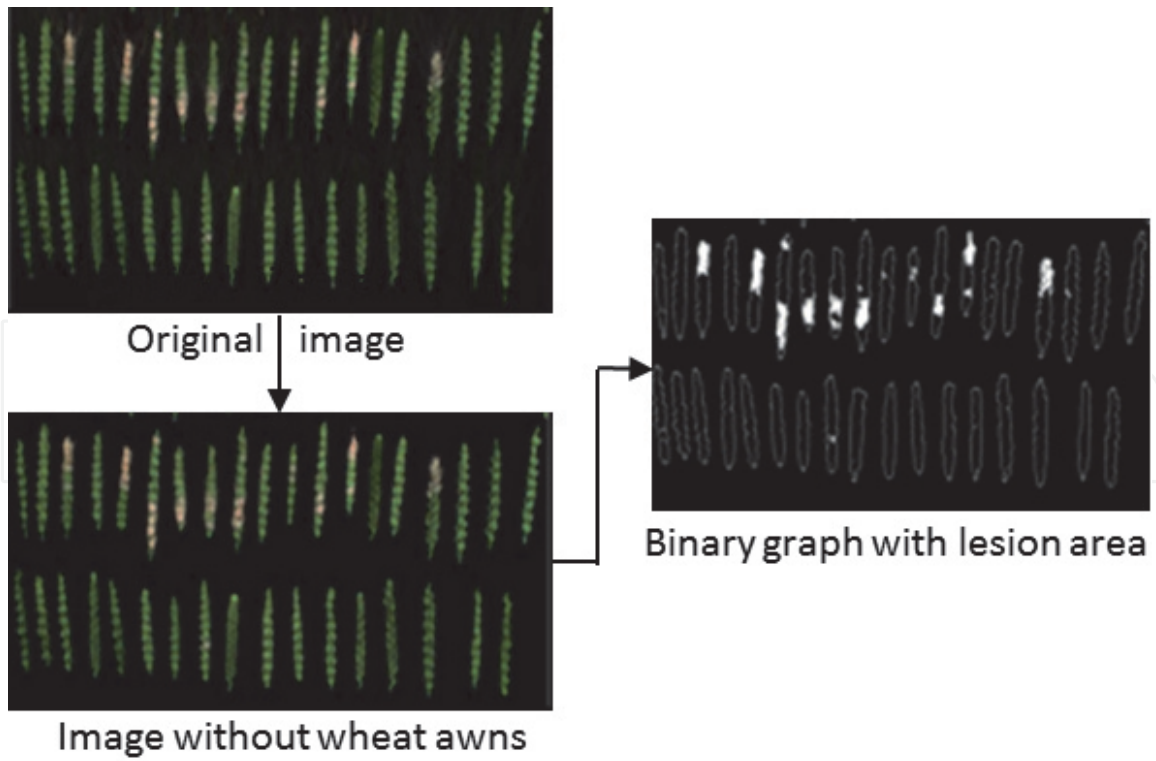


Figure 4. Extraction of diseased areas from wheat head: (A) wheat head image, (B) wheat head image with wheat awns removed, and (C) image of diseased areas extracted.

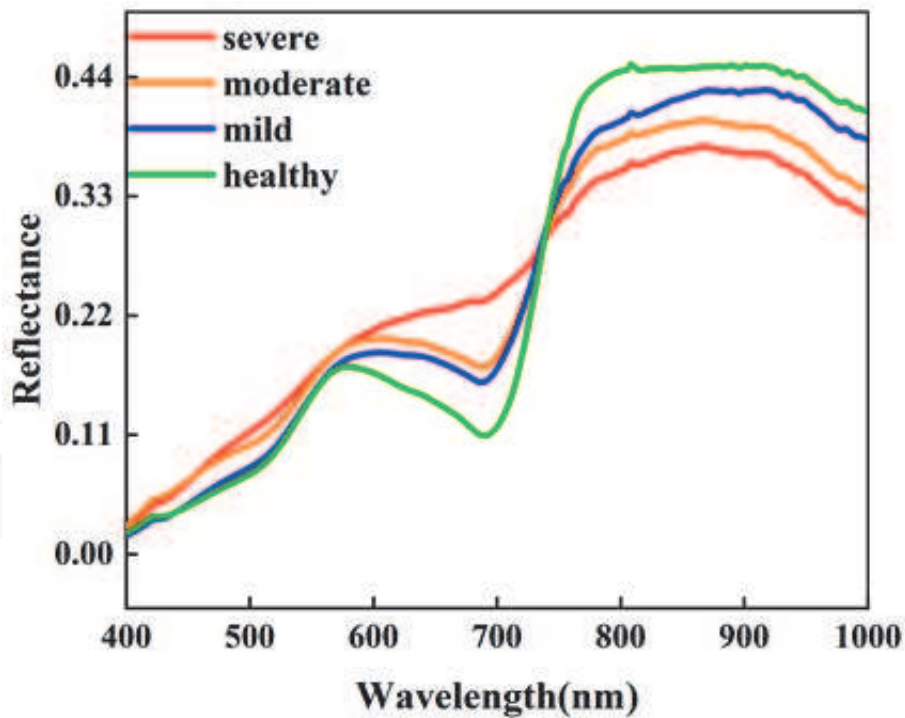


Figure 5. Spectral reflectance curves of wheat ears with different disease severities.

obvious green peak and red valley. Accordingly, these two spectral features disappear in the severely infected ears. Conversely, in the range of the 721–1000 nm band, the more severe the infected wheat ear the lower its reflectivity. The difference in responses of wheat ears with different severities in the bands of 550–720 nm and 721–1000 nm may be related to pigment and water content in mesophyll tissue [35]. Furthermore, with the increase of disease severity, the red edge position has a trend

towards shorter wavelengths. The above obvious spectral signature differences provide an important optical basis for analyzing and constructing the relationship between the spectral index and FHB severity in this work.

4.3 Prediction of FHB severity based on novel spectral disease index

4.3.1 Wheat material

The tested wheat cultivar was Xinong 979, moderately susceptible to the FHB disease. In this work, 149 and 229 wheat ears were collected at the late flowering (3 May 2018) and early filling (9 May 2018) stages for a total of 378 samples.

4.3.2 Characteristic band selection by random Forest

The algorithm of random forest (RF) was used to select the characteristic wavelengths that are sensitive to wheat FHB. The weight coefficients of all wavelengths were calculated in the spectral range of 400–1000 nm. To reduce the redundant information and maximize the effective spectral information, this work selected the wavelengths corresponding to the positive highest and negative lowest weight coefficients as the characteristic wavebands. As shown in **Figure 6**, the characteristic wavelengths were 570 nm and 678 nm at the late flowering stage, 565 nm and 661 nm at the early filling stage, and 560 nm and 663 nm at the combined stage.

4.3.3 Construction of proposed new spectral disease index for identifying wheat FHB

Previous studies [36, 37] have shown that the disease spectral index in the form of the normalized wavelength difference is very sensitive to spectral changes caused by powdery mildew, stripe rust, and aphids. Therefore, this work used the normalized wavelength difference in combination with characteristic wavelengths to construct the exclusive fusarium disease index (FDI) for each period. The formula is as follows.

$$FDI = \frac{R_{\lambda_1} - R_{\lambda_2}}{R_{\lambda_1} + R_{\lambda_2}} \quad (2)$$

where R_{λ_1} represents the reflectance at the λ_1 wavelength, and R_{λ_2} represents the reflectance at the λ_2 wavelength.

Here, with FDI as the independent variable and disease severity level (DSL) as the dependent variable, the relationship between FDI and DSL in different stages was

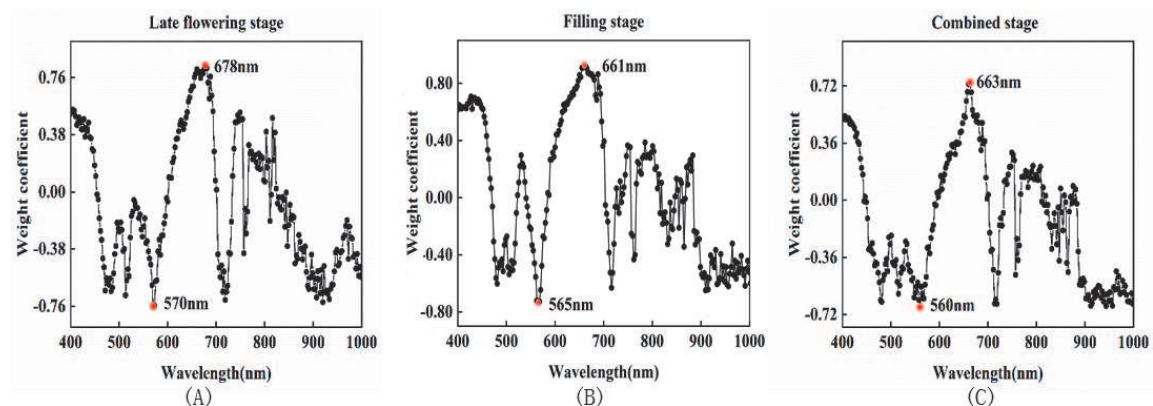


Figure 6. Weight coefficients calculated by RF at the late flowering (A), filling (B), and combined (C) stages.

evaluated by linear regression analysis (**Figure 7**). FDI made an accurate prediction of the DSL of wheat ears at the late flowering stage, filling stage, and combined stage (R^2 was greater than 0.90, RMSE was less than 0.08). At each stage, the R^2 and RMSE values of the training and test datasets were close, indicating that the model had a strong generalization ability. In addition, the prediction accuracy of FDI was the highest at the filling stage, followed by the late flowering stage and the combined stage.

In this work, the regression model obtained at the combined stage was applied to the test datasets at the late flowering and filling stages, respectively (**Figure 8**).

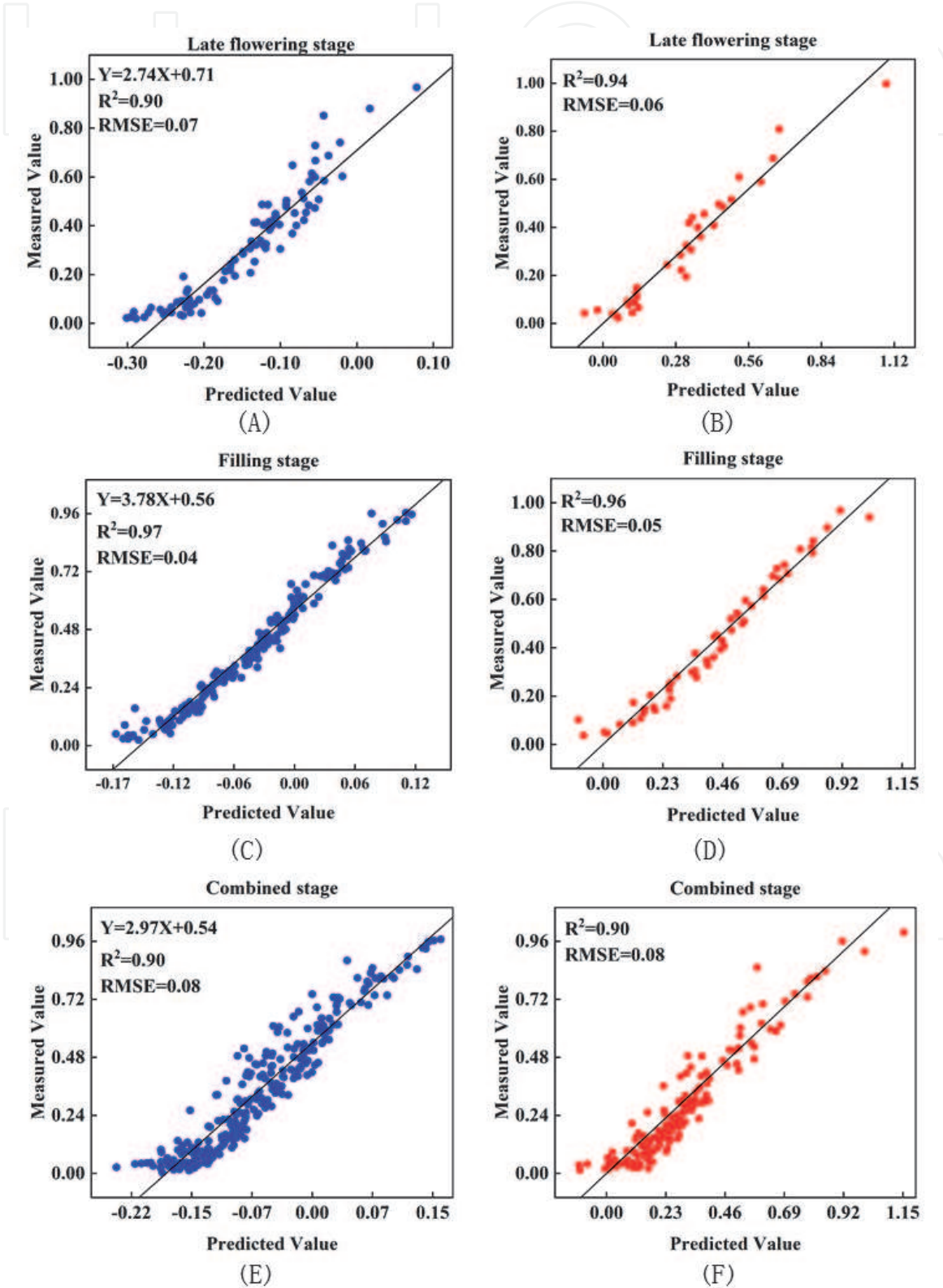


Figure 7. Regression models of the training datasets at the late flowering (A), filling (C), and combined (E) stages; and verification results of test datasets at the late flowering (B), filling (D), and combined (F) stages.

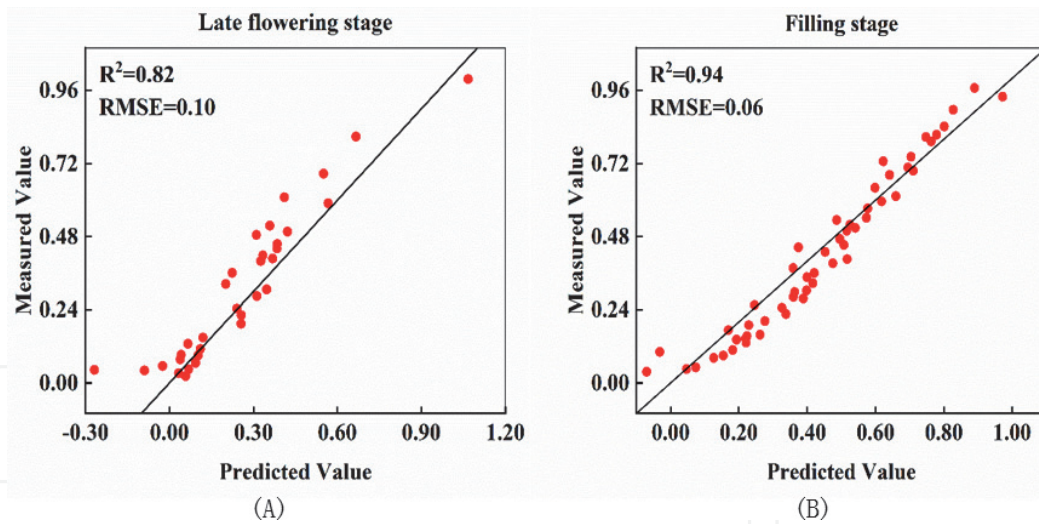


Figure 8.
Results of applying the regression model of the combined stage to test data of the late flowering stage (A), and the filling stage (B).

It was clear that the prediction accuracy of the model was close to that of the model established at the filling stage ($R^2 = 0.94$ and 0.96 , respectively), but lower than that of the model established at the late flowering stage ($R^2 = 0.82$ and 0.94 , respectively).

4.3.4 Comparison of FDI and commonly spectral index

Sixteen commonly used spectral indices were selected and compared with fusarium disease index (FDI) proposed in this work to evaluate the ability of FDI to identify and distinguish infected ears [38]. At the late flowering and combined stages, only FDI had an R^2 more than 0.9 in the training and test datasets. At the filling stage, only FDI and nitrogen reflectance index (NRI) had an R^2 above 0.9 in both the training and test datasets. The characteristic wavelengths of FDI (661 nm, 565 nm) and NRI (670 nm, 570 nm) were also close. The prediction accuracy of FDI to the disease severity was higher than that of other spectral indices at each stage, especially at the late flowering stage. Furthermore, transformed vegetation index (TVI), green index (GI), plant senescence reflectance index (PSRI), normalized difference vegetation index (NDVI), optimized soil-adjusted vegetation index (OSAVI), Lichtenthaler's indices (Lic1) performed relatively well at the late flowering and filling stages, but not at the combined stage. This may be attributed to the change of characteristic wavelengths at different growth stages.

4.4 Integrating spectral and image data to detect wheat FHB

4.4.1 Wheat material

Samples of 1,680 wheat ears with different levels of FHB severity, including the front side (defined as side A) and the reverse side (defined as side B) of wheat heads, were randomly collected from the healthy and infected samples in the research plots at the middle-to-late flowering (1 May 2019) and maturity (11 May 2019) stages.

4.4.2 Extraction process of spectral and image features

Spectral and image features of FHB were extracted from hyperspectral data of wheat ears (**Figure 9**). Spectral reflectance of each wheat ear was converted from the

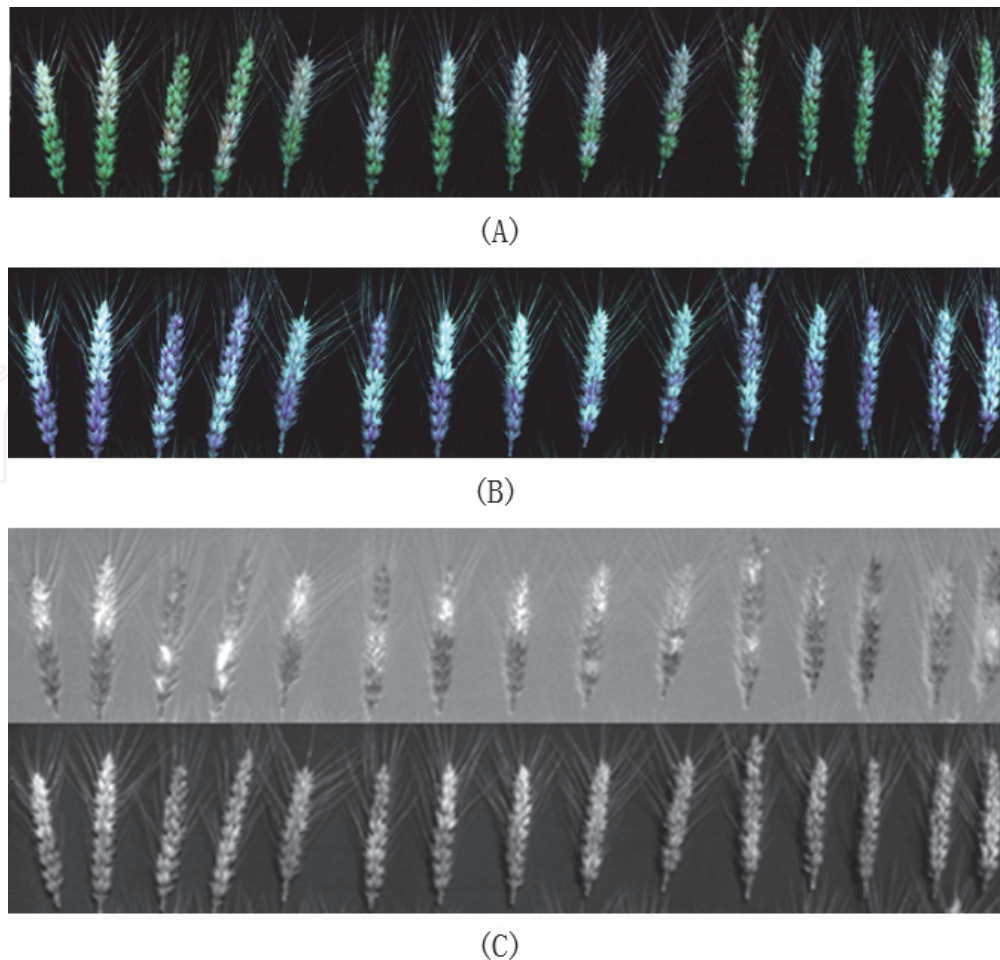


Figure 9.

Different feature images of wheat ears with FHB: (A) RGB image; (B) YDbDr image; and (C) images of the first second principal components (PC1-PC2).

intensity data of each sample using the ENVI 5.3 software (ITT Visual Information Solutions, Boulder, Utah, USA). Hyperspectral data has a large number of wavebands with information redundancy. Thus, principal component analysis (PCA) was used to reduce the high dimensional spectral data to a few principal components which can retain as much information as possible. The results showed that the first six principal components (PC1-PC6) explained over 98% of the variance and contained most of the information in the hyperspectral image.

Image information used for identifying wheat FHB were texture and color features. The work adopted gray level co-occurrence matrix (GLCM) and dual-tree complex wavelet transform (DTCWT) to obtain texture information of wheat FHB. The texture parameters based on GLCM contained energy, contrast, correlation, entropy and homogeneity calculated from four orientation values, respectively [39]. DTCWT can generate a quadtree structure, including two trees for the image rows and two trees for columns [40–42]. Color information was acquired from RGB images by computer vision technology. The RGB image was composed of red (660 nm), green (560 nm) and blue (480 nm) from hyperspectral images of wheat ears, and transferred to the YDbDr color space. Then, three moments were extracted from RGB and YDbDr space.

Spectral and image features obtained by above-mentioned methods were not all sensitive to wheat FHB. The algorithm of gradient boosting decision tree (GBDT) was used to select optimal features. GBDT is a common nonlinear model by scoring various features and removing the lowest score from features by the sequential backward elimination [43]. Finally, the number of optimum feature subsets was

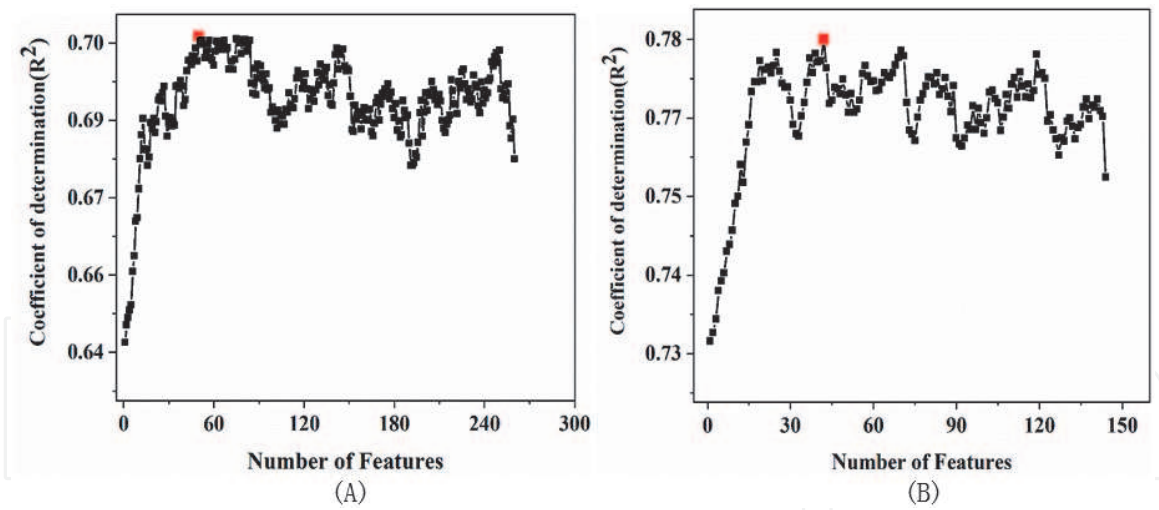


Figure 10.
 The relationship between the number of features and R^2 : (A) spectral characteristics in the side A of wheat ears, (B) image characteristics in the side A of wheat ears.

determined by the coefficient of determination (R^2) (**Figure 10**). The value of coefficient of determination (R^2) rose when the spectral features with the lowest scores were deleted (**Figure 10(A)**). Obviously, the model performance was improved due to redundant features being deleted. However, R^2 greatly decreased with the deletion of the useful features when the number of important features was reduced to one. For image features (**Figure 10(B)**), there was a similar trend to that of spectral features. Thus, the first 50 spectral and 40 image characteristics were selected from these features, respectively.

4.4.3 Identification of wheat FHB severity

The algorithm of random forest was used to establish the recognition model of wheat FHB with different patterns of feature combination (**Table 2**). The R^2 values of the models based on the spectral, image and fusion features increased successively. The performance of the model by spectral information was less effective than that of the model by image information for both sides of wheat ears. Even after reducing dimensions, the model with image features still had higher R^2 value and lower root mean square error (RMSE). However, the model constructed by the fusion features with spectral and image information provided the best performance, the R^2 values of which were 0.82 and 0.78 for data of side A and side B in wheat ears, respectively. Furthermore, the model by all data of side A and side B had R^2 of 0.89 and RMSE of 6.52 when using fusion features. It was indicated that the fusion

Features	Side A of wheat heads		Side B of wheat heads	
	R^2	RMSE	R^2	RMSE
Image	0.75	9.08	0.70	9.81
Spectral	0.68	10.25	0.63	10.98
Image- reduction	0.78	8.47	0.73	9.80
Spectral- reduction	0.70	10.30	0.64	11.70
Combined	0.82	7.98	0.78	8.46

Table 2.
 The prediction accuracy of random forest models with different features.

of spectral and image information can improve the performance of the identification model of FHB [44].

5. Hyperspectral monitoring of early powdery mildew in wheat

The detection and differentiation of powdery mildew at early stages not only allow timely fungicide treatment to reduce yield loss but also reduce fungicide usage to delay the build-up of fungicide resistance [45, 46]. Some studies have been conducted to evaluate the potential of using hyperspectral remote sensing to detect and quantify powdery mildew [47, 48]. The objective of our study was to construct a spectral disease index for early detection of powdery mildew in wheat.

5.1 Experiment and hyperspectral data acquisition

The experiment was conducted in a field located at the Beijing Academy of Agriculture and Forestry Science, China (39°56'N, 116°16'E). The cultivar of winter wheat used was 'jingshuang 16', highly susceptible to powdery mildew. This was a popular cultivar, and widely grown in China. Hyperspectral data were acquired from wheat leaves. Leaf samples were collected in the field at the filling stage and transported to a nearby laboratory for imaging spectrometer data measurement.

Imaging spectrometer data of leaves were obtained by the customized visible and near-infrared hyperspectral imaging system. The components of the system were shown in **Figure 11**. The spectral range of the system was between 400–1000 nm and its spectral resolution was 2.8 nm. The samples passed its view slot by the electric moving stage when the CCD camera was fixed over the stage. In this process, there were appropriate intensity of illumination and exposure time of the camera. Then, the images were acquired line-by-line.

Due to image noises in the wavebands with weak spectral response, spectral calibration was performed for the dark current correction to eliminate parts of the data noises. In addition, the spectral curve was normalized by band reflectance divided by the mean reflectance of the spectrum to suppress illumination changes among different measurements [49].

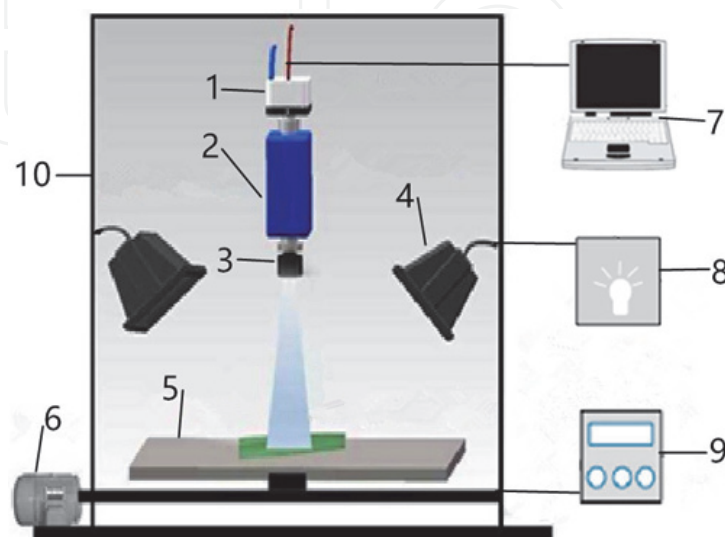


Figure 11.

The hyperspectral imaging system consisted of: (1) CCD camera, (2) imaging spectrograph, (3) lens, (4) light source, (5) sample stage, (6) electric moving stage, (7) computer, (8) light source controller, (9) moving stage controller, and (10) dark room.

5.2 Determination of disease index

Disease index (DI) was used to describe the levels of powdery mildew severity. The DI value of each leaf sample was determined by two processes. Firstly, the severity of wheat powdery mildew was estimated by the percentage of lesion area to whole leaf area and visual estimate of the percentage of infected leaf surface area on the leaf blade. Secondly, the estimated severity was divided into four categories to minimize human error for obtaining the disease index (DI), referring to Chinese Standard (NY/T 613–2002): 0–3% (no disease), 3%–10% (DI = 1), 10.1%–20% (DI = 2), and 20.1%–30% (DI = 3).

The calculation process of disease severity was shown in **Figure 12**, mainly including leaf area extraction and lesion region segmentation. By comparing the pixel values of a leaf blade in RGB color space, it was found that the pixel value of R component was the largest in the lesion area, while the pixel value of G component was the largest in the normal leaf area. Therefore, the ultra-red color feature 2R-G-B was selected for segmenting the normal leaf from other background (disease spots or insect injury). Images at 680 nm, 550 nm and 450 nm were synthesized pseudo color images. The automatic threshold of a component and b component in lab color space was set to extract the leaf area, and then the ultra-red color feature 2R-G-B was used to segment the disease spots on the leaves.

5.3 Construction of powdery mildew index (PMI) by the RELIEF-F algorithm

Powdery mildew index (PMI) consisted of a relevant single wavelength and a normalized wavelength difference. It was shown as the following formula.

$$PMI = \frac{R_1 - R_2}{R_1 + R_2} \pm 0.5R_3 \quad (3)$$

Where, R_1 and R_2 are reflectance in normalized wavelengths, and R_3 is reflectance in the most relevant single wavelength.

The most relevant single wavelength and normalized wavelengths were obtained by the RELIEF-F algorithm. The RELIEF-F algorithm was designed to measure how well attributes distinguished between instances within the close proximity of each

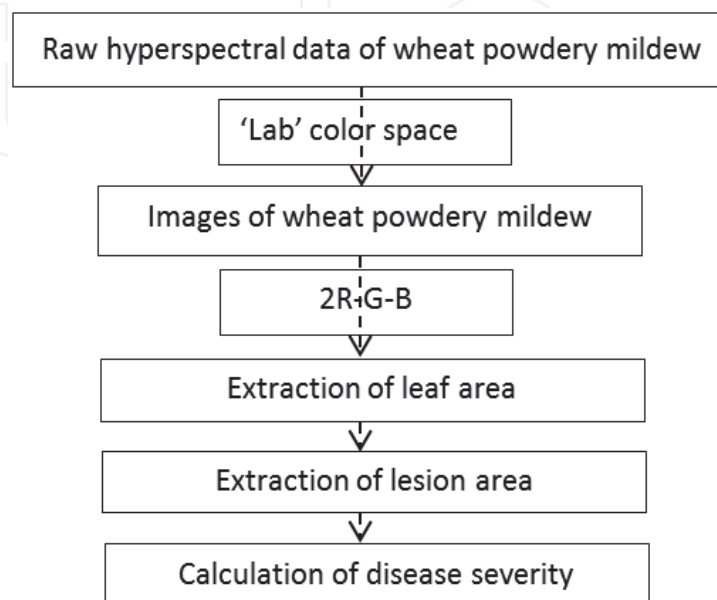


Figure 12.
The calculation process of disease severity.

other [50, 51]. Therefore, the algorithm was useful in finding some wavelengths for specific diseases. According to the study by Huang et al. [36], the most sensitive single wavelength was among wavelengths of the highest weighted (20%). Two normalized wavelengths were wavelengths from the best and worst weighted wavelengths (10%), respectively. And the distance between the two wavelengths was less than 50 nm.

5.4 Detection of early wheat powdery mildew by PMI

Figure 13 shows curves of normalized spectra and first-derivative spectra. The shapes of spectral curves of normal and diseased leaves for normalized spectra and derivative spectra were similar, but several differences existed in specific wavelength ranges among the three disease severity categories. At 450–700 nm, the reflectance value of normal leaves in red edge region had minimal value, followed by very slight and slight leaves had the highest value. At 750–1000 nm, normal leaves had highest reflectance value, followed by very slight leaves and slight leaves had lowest reflectance value. The more serious the disease was, the higher the

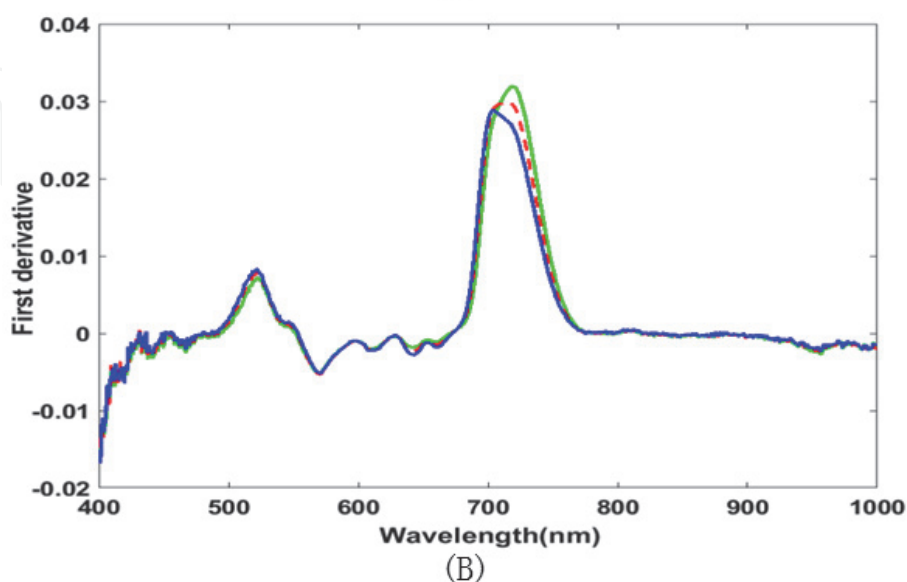
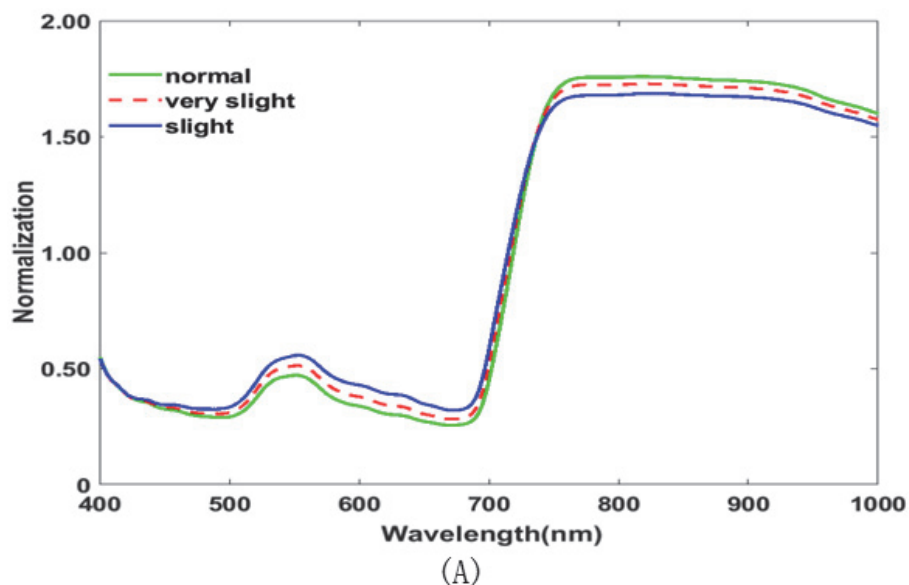


Figure 13.

Curves of normalized spectra and first derivative spectra. (A) Normalized reflectance curves of normal, very slightly-damaged (3% < lesion portion < 15%) and slightly-damaged leaves (15% lesion portion 30%); and (B) first derivative spectral curves of normal and diseased leaves.

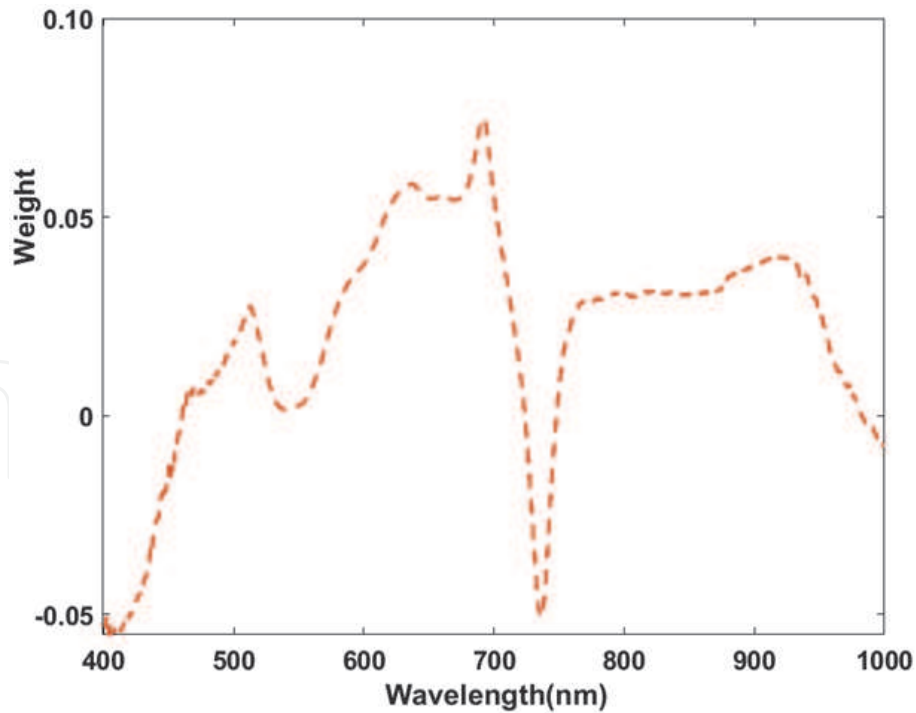


Figure 14.
 Single wavelength weights for regression analysis of PMI with disease severity.

reflectance of leaves in the visible region was, while the opposite was true in the near infrared region. These results were consistent with previous studies in meta-phase of powdery mildew [12, 52]. However, differences of the first derivative spectra between normal and diseased leaves were significant in the red edge region from 690 to 740 nm, but not obvious in the green edge region from 510 to 530 nm.

The curve of single wavelength weights is shown in **Figure 14**. Single wavelengths around 690, 820, and 910 nm had high relevance to diseased winter wheat

Ranking	Indices	Coefficient of correlation	Formula	Citation
1	PMI	0.90	$(R686 - R443)/(R686 + R443) - 0.5R913$	
2	NBNDVI	-0.86	$(R850 - R680)/(R850 + R680)$	[48]
3	ARI	0.85	$(R570 - R670)/(R570 + R670)$	[49]
4	PSRI	0.84	$0.5[120(R750 - R550) - 200(R670 - R550)]$	[50]
5	TVI	-0.77	$(R531 - R570)/(R531 + R570)$	[51]
6	MCARI	0.76	$(R550 - R531)/(R550 + R531)$	[51]
7	PRI	-0.76	$(\sqrt{(a670 + R670 + b)})/((a2 + 1)^{1/2}) - (R700/R670)$ $a = (R700 - R550)/150, b = R550 - (a - 550)$	[52]
8	CARI	0.72	$3[(R700 - R670) - 0.2(R700 - R550)(R700/R670)]$	[53]
9	TCARI	0.57	$[(R701 - R671) - 0.2(R701 - R549)]/(R701/R671)$	[54]
10	RVSI	0.56	$[(R712 + R752)/2] - R732$	[55]
11	PhRI	0.22	$(R680 - R500)/R750$	[56]
12	NRI	-0.17	$(R550)^{-1} - (R700)^{-1}$	[57]

R686 stands for reflectance at the band of 686 nm; and others stand for reflectance at their corresponding bands.

Table 3.
 Summary of correlation analysis between vegetation indices and DI [58–62].

leaves, and the normalized reflectance differences were around 445 and 680 nm. All possible wavelength combinations were calculated for the specific spectral index by the RELIEF-F algorithm. Finally, PMI for estimating DI was adopted based on reflectance at 913 nm and normalized reflectance difference between 443 and 686 nm. Statistical correlation analysis was carried out between PMI and DI. It was found that DI had a significant positive correlation to the PMI ($R^2 = 0.798$, $n = 70$). This indicates that the PMI had the potential for monitoring the early development of powdery mildew.

To compare the estimating ability of disease index between PMI and other hyperspectral vegetation indices, **Table 3** summarizes the results of correlation analysis between each of the 12 spectral features and DI. Of them, four indices had the coefficient of correlation more than 0.8, which were PMI, NBNDVI, ARI and PSRI. However, PMI had the highest value, indicating that PMI had powerful sensitivity to leaf powdery mildew.

6. Detection and diagnosis of wheat stripe rust

Wheat stripe rust (*P. striiformis* f. sp. *Tritici*) is one of the most destructive diseases of wheat worldwide, with characteristics of high prevalence, explosive occurrence, and severe damage at large areas. This disease is widespread in eastern and central Asia, western Europe and the Pacific coast of North America as well as Oceania, northern and eastern Africa, and south America. The infection process of the disease can be divided into the phases of contact, invasion, incubation, and occurrence. The spread of the spores in the subject cannot be observed by the naked eye during the incubation period. However, wheat stripe rust can easily become epidemic over a large area under suitable conditions once it enters the occurrence phase. Therefore, it is important to have a method that could rapidly and accurately detect stripe rust during the incubation period. Once it is detected, appropriate prevention and control measures could be taken before the disease spreads over a large area.

6.1 Microscopic image changes of wheat blades infected with stripe rust

Three leaf samples were collected and analyzed for obtaining microscopic images in this study. They were the infected blades at 8 days post inoculation (dpi), the diseased blades at 15 dpi, and the healthy blades as the controls. **Figure 15** depicts the reaction of wheat tissue at the different stages of stripe rust development in microscopic sections of primary infection sites. The healthy ones had a complete structure of crosscut sections, a compact structure and plentiful epidermal cells, and the chloroplasts were attached around the cell wall (**Figure 15 A1, A2 and A3**). When the blades were infected, the fungus would break through the protection of the epidermal cells to destroy the internal structure. Mesophyll cells were modified, and the number of chloroplasts was reduced considerably at 8 dpi (**Figure 15 B1, B2 and B3**). For the diseased blades (15 dpi), the fungus invaded each tissue of the blade and accumulated to create a large number of summer spore banks or spore beds (**Figure 15 C1, C2 and C3**).

6.2 Grading method of disease severity of wheat stripe rust using hyperspectral imaging technology

Identification and classification of wheat stripe rust plays an important role in managing this destructive disease to insure productivity of wheat. It helps to

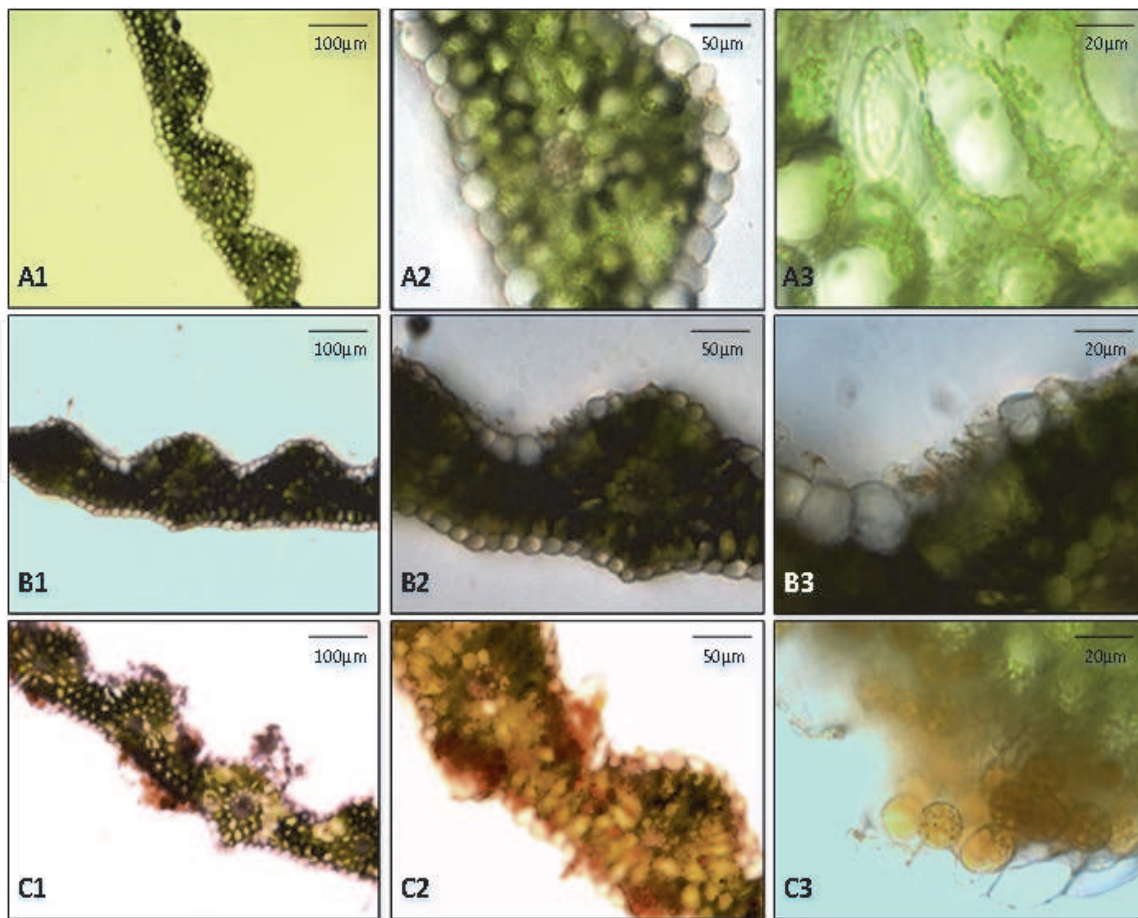


Figure 15. Sections of wheat leaf tissue infected with *Puccinia striiformis* f. sp. *tritici* at different stages of disease development: (A) healthy tissue, (B) tissue at the infection site at 8 days post inoculation (dpi) without macroscopic symptoms but with the epidermis layer destructed, and (C) chlorotic tissue with hyphae of the fungus.

quantitatively assess the level of wheat stripe rust severity in the field to develop strategies to achieve effective control of wheat stripe rust at early stages. Currently, estimation of severity of stripe rust is mainly relied on naked-eye observations. However, these methods are labor-intensive, time-consuming, besides requiring workers with high professional knowledge. In order to quickly and accurately evaluate the disease level of wheat stripe rust, a novel grading method based on hyperspectral imaging technology was proposed to determine severity levels of wheat stripe rust. Firstly, hyperspectral images were captured from 320 infected wheat leaf samples with different levels of disease severity and 40 healthy wheat leaf samples by a HyperSIS hyperspectral system covering the visible and near-infrared region (400 ~ 1000 nm). Secondly, via the analysis of spectral reflectance of leaf and background regions, there were obvious differences in spectral reflectance at the 555 nm wavelength. Therefore, the image of the 555 nm wavelength was named the feature image, which was manipulated by threshold segmentation to obtain a mask image. The logical and operation was conducted by using the original hyperspectral image and mask image to remove the background information. Thirdly, the principal component analysis (PCA) method was used for the dimension reduction of hyperspectral images. The operation results showed that the second principal component image (PC2) can significantly identify the stripe rust-infected area from the healthy area. Based on this, stripe rust-infected area was efficiently segmented by an Otsu method. Finally, the levels of wheat stripe rust severity was graded according to the proportion of stripe rust-infected area on the whole leaf area. To verify the effectiveness of the proposed method, a total of 270

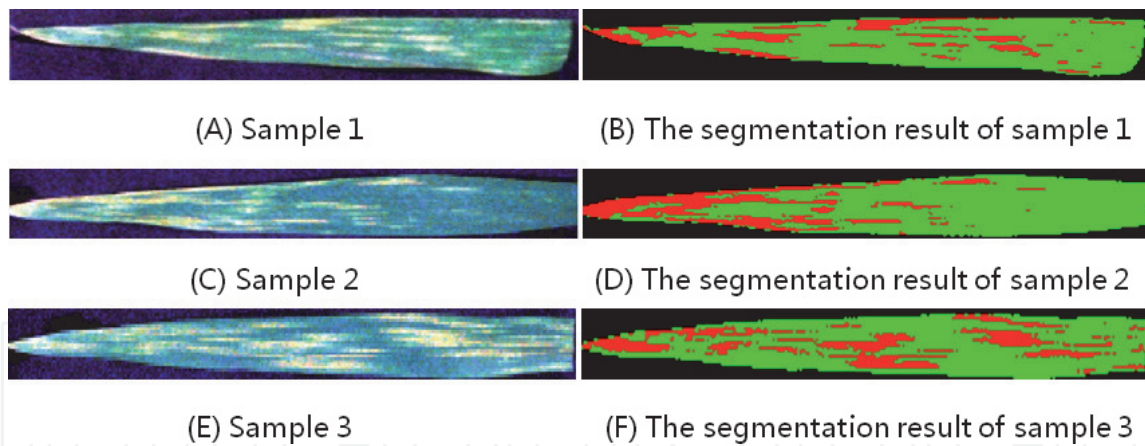


Figure 16.
Processing results of partial disease samples.

leaf samples were collected and evaluated. Experimental results showed that 265 samples could be accurately classified at different disease severities of wheat stripe rust and the overall classification accuracy was 98.15%. The treatment effect of some disease samples was shown in **Figure 16**. The results indicate that hyperspectral imaging technology has the potential to detect stripe rust in wheat.

7. Conclusion and prospects

In this article, we focus on using spectroscopy-based technology to explore developing innovative methods that are nondestructive, rapid, and accurate to diagnose and detect FHB, powdery mildew, and wheat stripe rust, three major fungal diseases in wheat worldwide. Based on their characteristic symptoms and disease development at different growth stages, we have proposed different detection methods and evaluated their performance. The conclusion is that spectroscopy technology can be used as an innovative tool for detection and monitoring of wheat diseases. However, the following limitations and challenges should be considered:

1. The experiments described in the current study are completed in the laboratory. Therefore, the stability and universality of diseased detection models developed from this study need to be further verified. Further field studies should be carried out to validate the model performance on different wheat cultivars and in different cropping areas.
2. Given the high levels of spread and severity the three wheat diseases pose, resulting in very limited window of time for action to control, it is very desirable to develop a detection method that is rapid and can cover a large area at a time. Integration of spectroscopy disease detection with UAV or satellite could be an effective approach toward this goal in the future efforts.
3. The high costs of spectroscopy sensors can also limit the potential application of this spectroscopy technology for disease detection. Future research efforts should be focused in designing a multispectral camera with a low price, improving image data processing speed, and developing methods that can detect multiple diseases simultaneously. In addition, it would be desirable to develop special disease detection device that is combined with the agricultural internet of things (IOT), agricultural situation investigation, and weather stations to detect crop diseases as quickly and accurately as possible, in the

form of multi-point investigation of smartphone terminals and fixed point collection in the frequently-occurring disease areas. These will provide important technical support for timely detection, monitoring, and control of wheat diseases.

IntechOpen

Author details

Fenfang Lin¹, Dongyan Zhang², Xin-Gen Zhou^{3*} and Yu Lei²


¹ School of Remote Sensing and Geomatics Engineering, Nanjing University of Information Science & Technology, Nanjing, China

² Anhui Engineering Laboratory of Agro-Ecological Big Data, Anhui University, Hefei, Anhui, China

³ Texas A&M AgriLife Research and Extension Center, Texas A&M University System, Beaumont, Texas, USA

*Address all correspondence to: xzhou@aesrg.tamu.edu

IntechOpen

© 2021 The Author(s). Licensee IntechOpen. This chapter is distributed under the terms of the Creative Commons Attribution License (<http://creativecommons.org/licenses/by/3.0>), which permits unrestricted use, distribution, and reproduction in any medium, provided the original work is properly cited. 

References

- [1] Shewry PR, Hey SJ. The contribution of wheat to human diet and health. *Food Energy Secur.* 2015; 4:178–202. DOI: <https://doi.org/10.1002/fes3.64>
- [2] FAO. Food and Agriculture Organisation of the United Nations, FAOSTAT, FAO Statistics Division. 2020. Available from <http://faostat.fao.org/site/567/default.aspx#ancor>
- [3] Roser M, Ritchie H, Ortiz-Ospina E. World population growth. Published online at OurWorldInData.org. 2013 Retrieved from: <https://ourworldindata.org/world-population-growth>
- [4] Godfray HCJ, Beddington JR, Crute IR, Haddad L, Lawrence D, Muir JF, Toulmin C. Food security: The challenge of feeding 9 billion people. *Science.* 2010; 327: 812–818. DOI: 10.1126/science.1185383
- [5] Juroszek P, Tiedemann A. Climate change and potential future risks through wheat diseases: a review. *Eur. J. Plant Pathol.* 2013; 136:21–33. DOI: 10.1007/s10658-012-0144-9
- [6] The World Bank. Reducing climate-sensitive risks. 2014. Available at <http://documents.worldbank.org/curated/en/486511468167944431/Reducing-climate-sensitive-diseaserisks>
- [7] Zhang JC, Huang YB, Pu RL, Gonzalez-Moreno P, Yuan L, Wu KH, Huang WJ. Monitoring plant diseases and pests through remote sensing technology: A review. *Comput. Electron. Agric.* 2019; 165:104943. DOI: 10.1016/j.compag.2019.104943
- [8] Karthikeyan L, Chawla I, Mishra AK. A review of remote sensing applications in agriculture for food security: Crop growth and yield, irrigation, and crop losses. *J. Hydrol.* 2020; 586:124905. DOI: 10.1016/j.jhydrol.2020.124905
- [9] Ali MM, Bachik NA, Muhadi N 'A, Yusof TNT, Gomes C. Non-destructive techniques of detecting plant diseases: a review. *Physiol. Mol. Plant Pathol.* 2019; 108: 101426. DOI: <https://doi.org/10.1016/j.pmpp.2019.101426>
- [10] Khaled AY, Aziz SA, Bejo SK, Nawi NM, Seman IA, Onwude DI. Early detection of diseases in plant tissue using spectroscopy – applications and limitations. *Appl. Spectrosc. Rev.* 2017; 53: 1–68. DOI: 10.1080/05704928.2017.1352510
- [11] Palacios SA, Erazo JG, Ciasca B, Lattanzio VMT, Reynoso MM, Farnochi MC, Torres AM. Occurrence of deoxynivalenol and deoxynivalenol-3-glucoside in durum wheat from Argentina. *Food Chem.* 2017; 230: 728–734. DOI: <https://doi.org/10.1016/j.foodchem.2017.03.085>
- [12] Zhang JC, Pu RL, Wang JH, Huang WJ, Yuan L, Luo JH. Detecting powdery mildew of winter wheat using leaf level hyperspectral measurements. *Comput. Electron. Agric.* 2012; 85:13–23. DOI: <https://doi.org/10.1016/j.compag.2012.03.006>
- [13] Ali S, Leconte M, Rahman H, Saqib MS, Gladieux P, Enjalbert J, De Vallavieille-Pope C. A high virulence and pathotype diversity of *Puccinia striiformis* f.sp. *tritici* at its centre of diversity, the Himalayan region of Pakistan. *Eur. J. Plant Pathol.* 2014a; 140: 275–290. DOI: <https://doi.org/10.1007/s10658-014-0461-2>
- [14] Ali S, Gladieux P, Leconte M, Gautier A, Justesen AF, Hovmøller MS, De Vallavieille-Pope C. Origin, migration routes and worldwide population genetic structure of the wheat yellow rust pathogen *Puccinia striiformis* f.sp. *tritici*. *PLoS Pathog.* 2014b; 10: e1003903. DOI: <https://doi.org/10.1371/journal.ppat.1003903>

- [15] Atta BM, Saleem M, Ali H, Bilal M, Fayyaz M. Application of fluorescence spectroscopy in wheat crop: early disease detection and associated molecular changes. *J. Fluoresc.* 2020; 30: 1–10. DOI: <https://doi.org/10.1007/s10895-020-02561-8>
- [16] Bürling K, Hunsche M, Noga G, Pfeifer L, Damerow L. UV-induced fluorescence spectra and lifetime determination for detection of leaf rust (*Puccinia triticina*) in susceptible and resistant wheat (*Triticum aestivum*) cultivars. *Funct. Plant Biol.* 2011; 38: 337–345. DOI: [10.1071/fp10171](https://doi.org/10.1071/fp10171)
- [17] Lüdeker W, Dahn HG, Günther KP. Detection of Fungal Infection of Plants by Laser-induced Fluorescence: An Attempt to Use Remote Sensing. *J. Plant Physiol.* 1996; 148: 579–585. DOI: [https://doi.org/10.1016/S0176-1617\(96\)80078-2](https://doi.org/10.1016/S0176-1617(96)80078-2)
- [18] Tischler YK, Thiessen E, Hartung E. Early optical detection of infection with brown rust in winter wheat by chlorophyll fluorescence excitation spectra. *Comput. Electron. Agric.* 2018; 146: 77–85. DOI: <https://doi.org/10.1016/j.compag.2018.01.026>
- [19] Padhye P, Rajani K. Machine vision guided system for classification and detection of plant diseases using support vector machine. *Int. J. Electron. Commun. Comput. Eng.* 2014; 5: 249–254.
- [20] Padmavathi K, Thangadurai K. Identification of plant leaves disease detection and optimal solution using genetic algorithm. *Int. J. Adv. Res. Comput. Sci. Softw. Eng.* 2015; 5: 1165–1168.
- [21] Johannes A, Picon A, Alvarez-Gila A, Echazarra J, Rodriguez-Vaamonde S, Navajas AD, Barredo AO. Automatic plant disease diagnosis using mobile capture devices, applied on a wheat use case. *Comput. Electron. Agric.* 2017; 138: 200–209. DOI: <https://doi.org/10.1016/j.compag.2017.04.013>
- [22] Wang H, Li G, Ma Z, Li X. Image recognition of plant diseases based on backpropagation networks. In: 2012 5th Int Congr Image Signal Process. 2012. p. 894–900. DOI: <https://doi.org/10.1109/CISP.2012.6469998>
- [23] Ngugi LC, Abelwahab M, Abo-Zahhad M. Recent advances in image processing techniques for automated leaf pest and disease recognition - a review. *Information Processing in Agriculture.* DOI: <https://doi.org/10.1016/j.inpa.2020.04.004>
- [24] Ferentinos KP. Deep learning models for plant disease detection and diagnosis. *Comput. Electron. Agric.* 2018; 145:311–318. DOI: <https://doi.org/10.1016/j.compag.2018.01.009>
- [25] Liu Z, Wu H, Huang J. Application of neural networks to discriminate fungal infection levels in rice panicles using hyperspectral reflectance and principal components analysis. *Comput. Electron. Agric.* 2010; 72: 99–106. DOI: <https://doi.org/10.1016/j.compag.2010.03.003>
- [26] Yuan L, Zhang J, Shi Y, Nie C, Wei L, Wang J. Damage mapping of powdery mildew in winter wheat with high-resolution satellite image. *Remote Sens.* 2014b; 6:3611–3623. DOI: [10.3390/rs6053611](https://doi.org/10.3390/rs6053611)
- [27] Huang W, Lamb DW, Niu Z, Zhang Y, Liu L, Wang J. Identification of yellow rust in wheat using in-situ spectral reflectance measurements and airborne hyperspectral imaging. *Precis. Agric.* 2007; 8: 187–197. DOI: [10.1007/s11119-007-9038-9](https://doi.org/10.1007/s11119-007-9038-9)
- [28] Zhang J, Pu R, Huang W, Yuan L, Luo J, Wang J. Using in-situ hyperspectral data for detecting and discriminating yellow rust disease from nutrient stresses. *Field Crop. Res.* 2012a;

134: 165–174. DOI: <https://doi.org/10.1016/j.fcr.2012.05.011>

[29] Bürling K, Hunsche M, Noga G. Presymptomatic detection of powdery mildew infection in winter wheat cultivars by laser-induced fluorescence. *Appl. Spectrosc.* 2012; 66: 1411–1419.

[30] Römer C, Bürling K, Hunsche M, Rumpf T, Noga G, Plümer L. Robust fitting of fluorescence spectra for pre-symptomatic wheat leaf rust detection with Support Vector Machines. *Comput. Electron. Agric.* 2011; 79: 180–188. DOI: <https://doi.org/10.1016/j.compag.2011.09.011>

[31] Iqbal MJ, Goodwin PH, Leonardos ED, Grodzinski B. Spatial and temporal changes in chlorophyll fluorescence images of *Nicotiana benthamiana* leaves following inoculation with *Pseudomonas syringae* pv. *tabaci*. *Plant Pathol.* 2012; 61: 1052–1062. DOI: 10.1111/j.1365-3059.2012.02592.x

[32] Scholes JD, Rolfe SA. Chlorophyll fluorescence imaging as tool for understanding the impact of fungal diseases on plant performance: a phenomics perspective. *Funct. Plant Biol.* 2009; 36: 880–892.

[33] Barbedo JG, Tibola CS, Fernandes JM. Detecting *Fusarium* head blight in wheat kernels using hyperspectral imaging. *Biosyst. Eng.* 2015; 131: 65–76. DOI: <https://doi.org/10.1016/j.biosystemseng.2015.01.003>

[34] Ravikanth L, Singh CB, Jayas DS, White ND. Classification of contaminants from wheat using near-infrared hyperspectral imaging. *Biosyst. Eng.* 2015; 135: 73–86. DOI: <https://doi.org/10.1016/j.biosystemseng.2015.04.007>

[35] Weber VS, Araus JL, Cairns JE, Sanchez C, Melchinger AE, Orsini E. Prediction of grain yield using

reflectance spectra of canopy and leaves in maize plants grown under different water regimes. *Field Crop Res.* 2012; 128: 82–90. DOI: 10.1016/j.fcr.2011.12.016

[36] Huang WJ, Guan QS, Luo JH, Zhang JC, Zhao JL, Liang D, Huang LS, Zhang DY. New optimized spectral indices for identifying and monitoring winter wheat diseases. *IEEE J. Sel. Top. Appl. Earth Obs. Remote Sens.* 2014; 7: 2516–2524. DOI: 10.1109/JSTARS.2013.2294961

[37] Mahlein AK, Rumpf T, Welke P, Dehne HW, Plümer L, Steiner U, Oerke EC. Development of spectral indices for detecting and identifying plant diseases. *Remote Sens. Environ.* 2013; 128: 21–30. DOI: <https://doi.org/10.1016/j.rse.2012.09.019>

[38] Zhang D, Wang Q, Lin F, Yin X, Gu C, Qiao H. Development and evaluation of a new spectral disease index to detect wheat fusarium head blight using hyperspectral imaging. *Sensors.* 2020a; 20:2260. DOI: 10.3390/s20082260

[39] Pourreza A, Pourreza H, Abbaspour-Fard MH, Sadrnia H. Identification of nine Iranian wheat seed varieties by textural analysis with image processing. *Comput. Electron. Agric.* 2012;83: 102–108. DOI: 10.1016/j.compag.2012.02.005

[40] Kingsbury N. Complex wavelets for shift invariant analysis and filtering of signals. *Appl. Comput. Harmon. A.* 2001; 10: 234–253. DOI: 10.1006/acha.2000.0343

[41] Selesnick IW, Baraniuk RG, Kingsbury NG. The dual-tree complex wavelet transform. *IEEE Signal Proc. Mag.* 2005; 22: 123–151. DOI: 10.1109/MSP.2005.1550194

[42] Yang P, Zhang FL, Yang GW. Fusing DTCWT and LBP based features

for rotation, illumination and scale invariant texture classification. *IEEE Access*. 2018; 13336–13349. DOI: 10.1109/ACCESS.2018.2797072

[43] Li TS, Wang J, Tu MS, Zhang Y, Yan YH. Enhancing link prediction using gradient boosting features. *Intelligent Computing Theories and Application, Ictic 2016*. 2016; 9772: 81–92. DOI: 10.1007/978-3-319-42294-7_7

[44] Zhang D, Chen G, Yin X, Hu R, Gu C, Pan Z, Zhou X, Chen Y. Integrating spectral and image data to detect *Fusarium* head blight of wheat. *Comput. Electron. Agric.* 2020b; 175: 105588. DOI: <https://doi.org/10.1016/j.compag.2020.105588>

[45] Sankaran S, Mishra A, Ehsani R, Davis C. A review of advanced techniques for detecting plant diseases. *Comput. Electron. Agric.* 2010; 1: 1–13.

[46] Jafari M, Minaei S, Safaie N, Torkamani-Azar F. Early detection and classification of powdery mildew-infected rose leaves using ANFIS based on extracted features of thermal images. *Infrared Phys. Technol.* 2016; 76: 338–345.

[47] Lin FF, Wang DD, Zhang DY, Yang XD, Yin X, Wang DY. Evaluation of spectral disease index PMI to detect early wheat powdery mildew using hyperspectral imagery data. *Int. J. Agric. Biol.* 2018; 20: 1970–1978. DOI: 10.17957/IJAB/15.0716

[48] Huang LS, Zhang Q, Zhang DY, Lin FF, Chao X, Zhao JL. Early diagnosis of wheat powdery mildew using Relief-F band screening. *Infrared and Laser Engineering*. 2018; 47: 210–217.

[49] Pu R, Kelly M, Chen Q, Gong P. 2008. Spectroscopic determination of health levels of coast live oak (*Quercus agrifolia*) leaves. *Geocarto Int.* 2008; 23: 3–20.

[50] Kira K, Rendell L. A practical approach to feature selection. *Proc. 9th Int. Workshop Mach. Learn.*, San Mateo, CA, USA. Morgan Kaufmann Publishers Inc; 1992. P. 249–256.

[51] Robnik-Sikonja M, Kononenko I. Theoretical and empirical analysis of ReliefF and RReliefF. *Mach. Learn.* 2003; 53: 23–69.

[52] Huang LS, Zhang DY, Liang D, Yuan L, Zhao JL, Hu GS, Du SZ Xu XG. Continuous wavelet analysis for diagnosing stress characteristics of leaf powdery mildew. *Int. J. Agric. Biol.* 2013; 15: 34–40. DOI: 10.1684/agr.2012.0578

[53] Thenkabail PS, Smith RB, De Pauw E. Hyperspectral vegetation indices and their relationships with agricultural crop characteristics. *Remote Sens. Environ.* 2000; 2: 158–182. DOI: [https://doi.org/10.1016/S0034-4257\(99\)00067-X](https://doi.org/10.1016/S0034-4257(99)00067-X)

[54] Filella I, Serrano L, Serra J, Penuelas J. Evaluating wheat nitrogen status with canopy reflectance indices and discriminant analysis. *Crop Sci.* 1995; 5: 1400–1405.

[55] Broge NH, Leblanc E. Comparing prediction power and stability of broadband and hyperspectral vegetation indices for estimation of green leaf area index and canopy chlorophyll density. *Remote Sens. Environ.* 2001; 2: 156–172. DOI: [https://doi.org/10.1016/S0034-4257\(00\)00197-8](https://doi.org/10.1016/S0034-4257(00)00197-8)

[56] Gamon JA, Penuelas J, Field CB. A narrow-waveband spectral index that tracks diurnal changes in photosynthetic efficiency. *Remote Sens. Environ.* 1992; 1: 35–44. DOI: [https://doi.org/10.1016/0034-4257\(92\)90059-S](https://doi.org/10.1016/0034-4257(92)90059-S)

[57] Kim MS, Daughtry CST, Chappelle EW, McMurtrey JE. The use of high spectral resolution bands for estimating absorbed photosynthetically

active radiation (APAR). Proc. 6th Int. Symposium on Physical Measurements and Signatures in Remote Sensing. France Val d'Isere; 1994. P. 299–306.

[58] Haboudane D, Miller JR, Pattery E, Zarco-Tejad PJ, Strachan IB. Hyperspectral vegetation indices and novel algorithms for predicting green LAI of crop canopies: Modeling and validation in the context of precision agriculture. *Remote Sens. Environ.* 2004; 3: 337–352. DOI: <https://doi.org/10.1016/j.rse.2003.12.013>

[59] Daughtry CS, Walthall CL, Kim MS, de Colstoun EB, McMurtrey JE. Estimating corn leaf chlorophyll concentration from leaf and canopy reflectance. 2000. *Remote Sens. Environ.* 2000; 2: 229–239. DOI: [https://doi.org/10.1016/S0034-4257\(00\)00113-9](https://doi.org/10.1016/S0034-4257(00)00113-9)

[60] Merton R, Huntington J. Early simulation of the ARIES-1 satellite sensor for multi-temporal vegetation research derived from AVIRIS. Summaries of the Eight JPL Airborne Earth Science Workshop, Pasadena, CA: JPL, Publication; 1999. P. 299–307.

[61] Merzlyak MN, Gitelson AA, Chivkunova OB, Rakitin VY. Non-destructive optical detection of pigment changes during leaf senescence and fruit ripening. *Physiol. Plant.* 1999; 1: 135–14. DOI: [10.1034/j.1399-3054.1999.106119.x](https://doi.org/10.1034/j.1399-3054.1999.106119.x)

[62] Gitelson A, Merzlyak MN, Chivkunova OB. Optical properties and nondestructive estimation of anthocyanin content in plant leaves. *Photochem. Photobiol.* 2001; 1: 38–45. DOI: [10.1562/0031-8655\(2001\)074<0038:opaneo>2.0.co;2](https://doi.org/10.1562/0031-8655(2001)074<0038:opaneo>2.0.co;2)